RSC Mechanochemistry

ROYAL SOCIETY OF CHEMISTRY

PAPER

View Article Online
View Journal | View Issue

Cite this: *RSC Mechanochem.*, 2026, **3**, 273

Mechanochemical synthesis of bent metallacycles and confinement catalysis in the solid-state

Peiyi Wang, Shi Li, Fang-Zi Liu and KaKing Yan *

Synthetic cages or capsules serve as versatile container molecules capable of facilitating host–guest chemistry and confinement-driven catalysis, akin to natural enzymes. However, their guest-binding cavities are typically formed concurrently with their discrete frameworks. In this study, we demonstrate that bent metallacycles, Pd_2L_2, structurally analogous to partial constructs of discrete coordination capsules Pd_2L_4, can be effectively synthesized mechanochemically. Crystallographic analysis revealed that these structures would self-assemble into non-covalent coordination capsules with tunable interior cavity dimensions. They were further utilized in solid-state, confinement-directed C–C bond formation catalysis, where they exhibited enhanced substrate size/shape recognition capabilities, compared to common organic base catalysts.

Received 7th June 2025
Accepted 13th November 2025

DOI: 10.1039/d5mr00075k

rsc.li/RSCMechanochem

Introduction

Macrocycles play a central role in supramolecular chemistry, as evidenced by their connection with two Nobel Prizes in Chemistry,[1,2] awarded in 1987 and 2016. These structures,[3–7] exemplified by notable systems such as natural valinomycin and synthetic counterparts like crown ethers, exhibit distinctive guest-association properties that are critical for applications such as separation,[8] drug delivery,[9] and catalysis.[10] Despite their significance, macrocycle synthesis has historically been challenging. In 1990, Fujita and co-workers introduced a coordination-driven approach, enabling the synthesis of a palladium-based macrocycle in the absence of a template and dilution conditions, in quantitative yield.[11] This extraordinarily efficient solution-based method fundamentally transformed the field.[12]

In recent years, due to their environmental friendliness, mechanochemical approaches have garnered significant attention in all branches of chemical synthesis,[13,14] such as organic, organometallic, as well as supramolecular self-assembly processes. Otera and co-workers provided an early mechanochemical metallacycle example of a Fujita-type Pt_4L1_4 (**L1** = 4,4′-bipyridine) *via* hand grinding.[15,16] More recently, our group reported the construction of two Pd-based metallacycles, Pd_2L1_2 and Pd_2L2_2 (**L2** = 1,3,5-tris(1-imidazolyl)benzene), by ball-milling methods, which are inaccessible through conventional solvent-based methods.[17] While these studies highlight the synthetic advantages of mechanochemistry, metallacycles' functions under mechanochemical conditions, especially in enzyme-mimic catalysis are completely unexplored in the literature.

In practice, supramolecular confinement catalyses are more suited to molecular cages, *e.g.* Pd_2L_4 (**1**), as they possess well-defined hydrophobic cavities crucial in molecular recognition and host–guest molecular information transfer.[18] However, is a discrete cage or capsule really necessary to facilitate micro-environment catalysis? Could a guest-binding cavity be created *in situ* with fragments of a cage in the presence of substrates? In this work, by molecular design, we show that bent metallacycles Pd_2L_2 (**2**) (**L** = **L3**: 2,7-bis(3-pyridyl)naphthalene or **L4**: 1,3-bis(3-pyridyl)benzene), structurally-related fragments of discrete

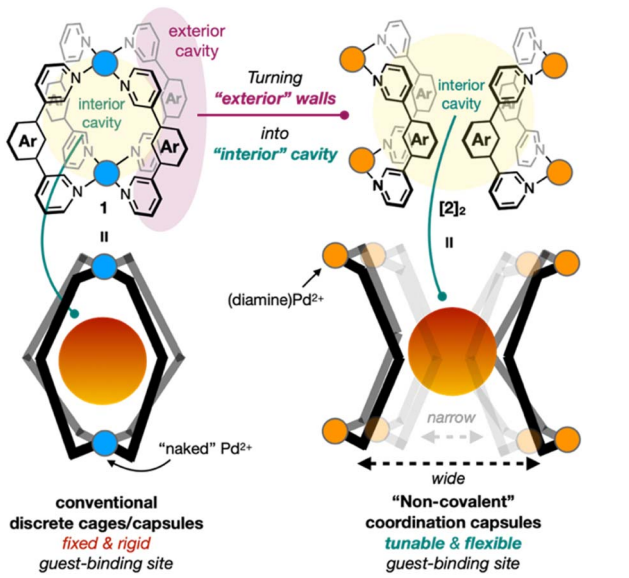

Fig. 1 The inspiration and design principle in this work. The goal is to turn the "exterior" walls in rigid capsule **1** in solution into a more flexible "interior" cavity of $[2]_2$ that is self-assembled in the solid-state by **2**, a metallacyclic fragment of **1**.

School of Physical Science and Technology, ShanghaiTech University, 201210 Shanghai, China. E-mail: yankk@shanghaitech.edu.cn

capsule **1**, could be turned "outside-in" to create non-covalent coordination capsules with tunable interior cavity dimensions (Fig. 1). These materials engage in efficient supramolecular confinement catalysis in the solid-state with the help of mechanical stimulation. More interestingly, they exhibit enhanced substrate size recognition catalysis, a hallmark feature in enzymes, compared to common organic base catalysts.

Results and discussion

2a can be conveniently prepared from (tmeda)Pd$(NO_3)_2$ in the presence of 1 equiv. of **L3** in excellent yield (89%) under solventless milling conditions (Fig. 2).[19] The formation of **2a** was confirmed by both NMR and ESI-mass spectroscopy. Employing a similar ball-milling strategy, other metallacycles $\mathbf{Pd_2L_2}$ can be conveniently produced in high yields, for example with **L3** and **Pd** = (eda)Pd (**2b**) (eda = ethylenediamine) or (1*R*,2*R*-cdm)Pd (**2c**) (1*R*,2*R*-cdm = (1*R*,2*R*)-1,2-cyclohexanediamine); or tmedaPd$(NO_3)_2$ and **L4** to give a phenyl backbone-based $\mathbf{Pd_2L4_2}$ (**2d**) (Fig. 2). These $\mathbf{Pd_2L_2}$ species were fully-characterized by standard ^{1}H and ^{13}C NMR spectroscopy, as well as ESI-MS and single crystal X-ray diffraction (sc-XRD) (**2a** and **2d**) (Fig. 2).

The dinuclear $\mathbf{Pd_2L_2}$ bowl shape-like *cis*-conformation of **2a** and **2d** was unambiguously confirmed by a sc-XRD study (Fig. 2). In both solid-state structures, one NO_3^- group was located at the center of the metallacycle framework. The anionic binding is revealed by multiple CH···O interactions between the α-C–H of pyridyls, C–H of tmeda and O in NO_3^-, stabilizing the formation of an anion-binding inclusion complex. Since the interactions do not involve any π-type interactions with either the pyridyl group or the naphthyl backbone, the NO_3^- capture is likely to be electrostatic in nature. Besides, the bent structures in both cases are worthy of further discussion. Pd-coordination with **L3** creates an L-shaped metallacyclic structure with a Np-(Pd-Pd)$_{centriod}$-Np angle of 75.6° for **2a**, while the corresponding angle in **2d** is significantly more obtuse at 105.8°. In comparison, the through-space angle of $\mathbf{Pd_2L2_2}$ derived from timb (timb = 1,3,5-tris(imidazyl)benzene) is even wider at 125°.[17b] These analogous structures provide a key clue that the bent angle, representing a direct relationship to the dimension of a potential guest binding site, could be systematically tuned by rational design.[20]

It has been demonstrated previously that coordination complexes could self-assemble in the solid state into well-defined higher ordered molecular capsules.[21] Sun reported an elegant template-facilitated self-assembly of porous hexameric cage-like aggregates with lanthanide-based triply helicates, which is capable of chiral guest recognition.[22] When we carefully examined the crystal packing structures of both **2a** and **2d**, a self-driven ordering of $\mathbf{Pd_2L_2}$ into capsule-like units, $[\mathbf{Pd_2L_2}]_2$ was identified (Fig. 3). For example, **2a** is packed in the crystal in such a way that units A and B or C and D are aligned in a capsule-like orientation with a $C_{(Np–Np)centroid}$ to $D_{(Np–Np)centroid}$

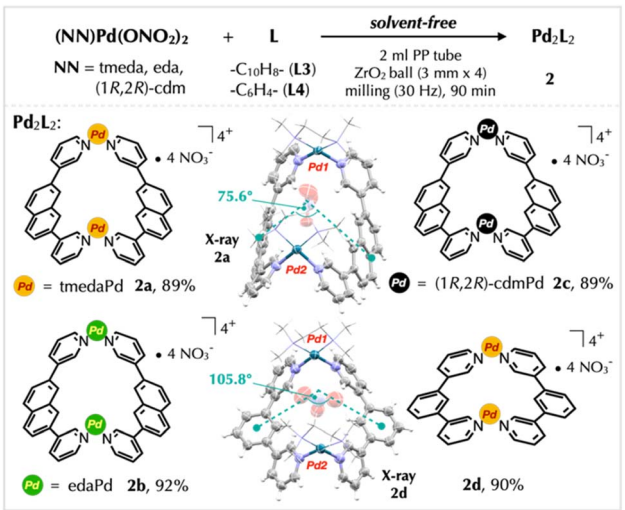

Fig. 2 The solid-state synthetic route to various $\mathbf{Pd_2L_2}$ metallacycles (**2a–d**), and their corresponding crystal structures (**2a** and **2d**). The macrocycle bent degrees were obtained from the Np (centroid)-Pd_2-centriod-Np (centroid) angle and the Ph (centroid)-Pd_2-centriod-Ph (centroid) angle, and they are labeled in green. The molecular structures of **2a** and **2d** with thermal ellipsoids drawn at 50% probability. Only the encapsulated nitrate groups are shown.

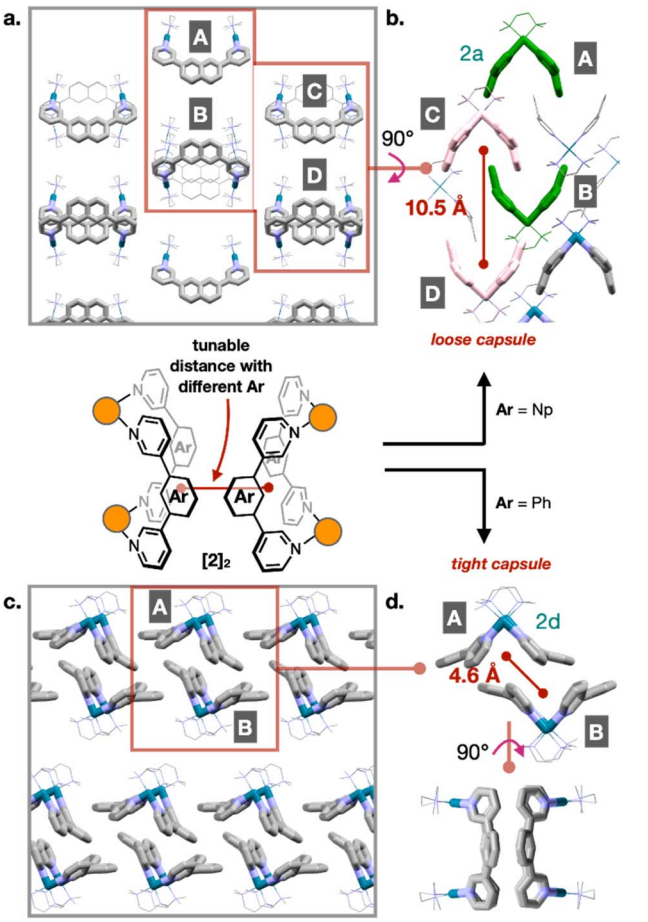

Fig. 3 X-ray crystal packing structures of (a and b) **2a** and (c and d) **2d**, and our hypothetical $[2]_2$ model illustrating the tunability of the cavity distance by varying the aryl linker in the ligand.

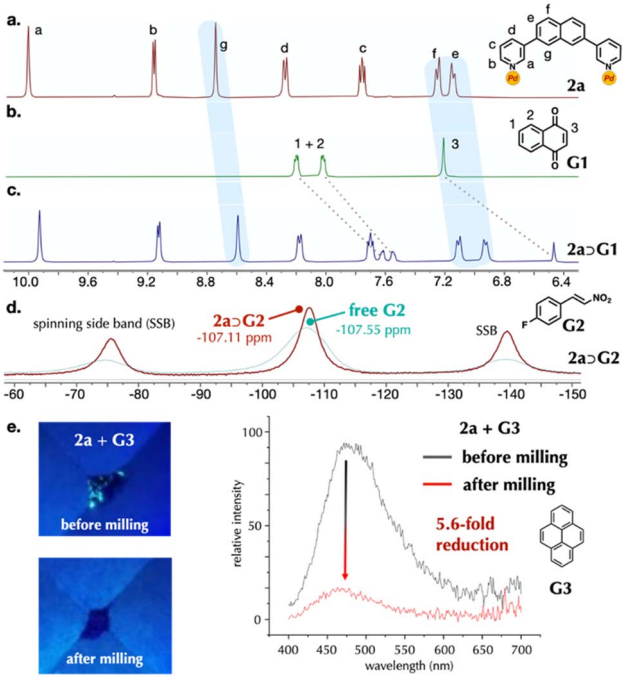

Fig. 4 (a–d) ^{1}H NMR spectra obtained in a mixed solvent of $CD_3CN/D_2O = 1:4$ (10 mM) of (a) **2a**; (b) **G1**; and (c) host–guest complexation between **2a** and **G1**. Blue highlights and dotted lines illustrate the resonance shift of **2a** and **G1** upon complexation with **G1**, respectively. (d) Solid-state ^{19}F NMR spectra of free **G2** (red line) and inclusion complex from **2a** and **G2** (green line). (e) (Left) Photograph of solid samples of (from top to bottom) **2a** + **G3**: before milling and after stirring, under 365 nm UV-light irradiation, and (right) solid state emission turn OFF of **2a** + **G3** upon ball-milling treatment.

distance of 10.5 Å (Fig. 3b). Meanwhile, the capsular structure is much easier to recognize in that of **2d**, where two molecules of **2d** are in close proximity, face-to-face to each other, with an $A_{(Ph-Ph)centroid}$ to $B_{(Ph-Ph)centroid}$ distance of only 4.6 Å (Fig. 3c and d). These packing structures offer a glimpse at something more crucial. That is, by applying different ligand linkers, the "tightness" of the $[2]_2$ unit and its cavity size or shape, in principle, can be designed and tuned, potentially for guest binding reactions.

At the onset, the guest-binding aspect of **2** in solution was investigated. For example, addition of 1,4-naphthoquinone (**G1**) in a solution ($CD_3CN/D_2O = 1:4$) of **2a** induced an obvious up-field shift in guest resonances, up to 0.7 ppm (Fig. 4c). Moreover, upon inspecting the resonance changes in **2a**, its naphthyl core experienced the most pronounced influence, implying that guest molecules are located within the L-shaped binding pocket created by **2a**. In addition, the host–guest association event was also confirmed by DOSY experiments (Fig. S31).

Our group has a long-standing interest in investigating coordination self-assembly and host–guest chemistry under solvent-free mechanochemical conditions. Solid-state ^{19}F NMR spectrum was employed to evaluate the guest binding ability of **2** in the solid-state. The ^{19}F NMR spectrum of a milled sample of **2a** and 4-fluoro-β-nitrostyrene (**G2**) revealed a 0.44 ppm shift in guest F-resonance upon mixing with **2a** (Fig. 4d),[23–25] providing strong support for host–guest complexation between **2a** and **G2** in the solid-state. Attempts to obtain single crystals of the complexation species with **2** failed, presumably due to the relatively weak binding affinity in solution.

To strengthen the evidence that **2** is a capable host for guest molecule entrapment, especially in the solid-state, we undertook photophysical experiments using metallacycle **2a** with pyrene (**G3**), which displays distinctive aggregation-induced emission (AIE) arising from the excimer formation in the solid state. However, fluorescence of **G3** is quenched in solution due to the lack of self-aggregation.[26] When **2a** with **G3** (forming complex $(\mathbf{2a})_n \supset (\mathbf{G3})_n$) was subjected to ball-milling treatment, the inherent fluorescence of **G3** in the solid state was much diminished, showing over a 5.6-fold reduction (turn OFF) compared to the unmilled mixture (Fig. 4e). Even more surprising was the observation that **2d**, which features a highly congested cavity, also effectively quenched the emission of **G3** (Fig. S45). This suggests a degree of cavity flexibility that permits guest accommodation. Since mechanical milling is necessary to trigger encapsulation, we conclude that mechanical stimulation is a prerequisite for inducing pore opening in **2d**, a material otherwise classified as non-porous based on its static crystal structure. In addition, powder X-ray diffraction (PXRD) was also applied to provide bulk structural information on **2a** with **G2**. While the structure of a milled sample of **2a** remained crystallographically intact, co-milling with **G2** (presumably formation of $(\mathbf{2a})_n \supset (\mathbf{G2})_n$) resulted in a featureless PXRD spectrum. The experimental observation supported that **G2** engages in intermolecular interaction with **2a** in the solid state upon mechanical impact (Fig. S46). As the mechanical impact takes place at the crystal interface between **2a** and **G2**, the mechanical stimulus-triggered phase transformation is expected to distribute locally, resulting in amorphous solids. Such mechanical impact-induced reaction behavior was previously observed and proposed by Ito with an Au(I) complex.[27] Upon mechanical triggering, a chain-like process is initiated from the point of impact at the surface extending towards the inner layers of the solid structure. Subsequently, we believe, it will increase the effective surface area of **2a**, inducing reagent access to the reaction domain. Collectively, although a molecular level understanding of the guest binding mode and the mechanism of force-induced cavity opening in **2** is currently lacking in this work, the limited mechanistic data obtained suggest that **2** is fully capable of hosting guest molecules. More importantly, **2** is well-poised to engage in supramolecular catalysis in the solid-state.

Michael addition reaction is a classic organic transformation to construct a C–C bond between a nucleophile and a Michael acceptor. In general, the reactions are often facilitated by common bases and both Lewis and Bronsted acids.[28] Lately, these reactions were also studied with coordination cage catalysts under aqueous conditions, notably by the work of Mukherjee[29] and Lusby,[30] yet analogous solid-state counterparts are lacking in the literature.

When a mixture of 4-chloro-β-nitrostyrene (**3a**) and an equivalent of dimethylbarbituric acid (**4**) was charged into a 2 mL polypropylene (PP) tube with ZrO_2 milling balls (3 mm ×

Table 1 Reaction screening in mechanochemical Michael addition between **3a** and **4**

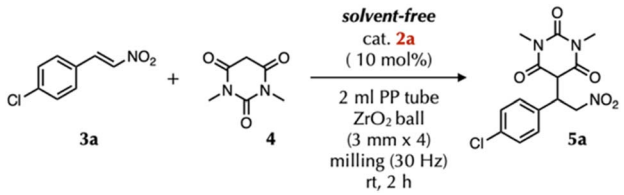

Entry	Deviation from above conditions	NMR yield[a] (%) of **5a**
1	None	98
2	30 Hz, 1 h	90
3	20 Hz, 2 h	73
4	5 mm × 1	93
5	Milling at 0 °C	43
6	Milling at −30 °C	27
7	1 (or 5) mol% **2a**	51(88)
8	10 mol% **2b**	54
9	10 mol% **2c**	93
10	10 mol% **2d**	96
11	10 mol% $\mathbf{Pd_2L3_4}$ cage (**1**)	65
12	No **2a**	9
13	10 mol% (tmeda)$Pd(NO_3)_2$ or $(py)_2PdCl_2$ as the catalyst	2 or 9
14	20 mol% **L3** or **L4**	93 or 92
15	With (or without) **2a** in DMSO-d_6	71(59)[b]

[a] Yields determined by ^{1}H NMR spectroscopy with 1,3,5-trimethoxybenzene as an internal standard. [b] Reaction with (without) **2a** in CD_3CN/D_2O (1 : 4) gave **5a** in 63% (61%) yield.

4) in the presence of **2a** (10 mol%), the solid sample was subjected to a mixer mill set at 30 Hz for 2 h. After the reaction, the milled sample was analyzed by ^{1}H NMR spectroscopy. The C–C bond coupling product (**5a**) was obtained in an excellent 98% yield (Table 1, entry 1). Without **2a**, the solid-state background reaction is negligible (9% yield of **5a** under the same mechanochemical condition) (entry 12). Reducing the milling frequency or reaction time led to lower conversions (entries 2–3). Using a larger milling ball (5 mm) instead would have had a slight diminishing effect on reaction efficiency (entry 4). Interestingly, the mechanochemical reactions could still proceed at as low as −30 °C, suggesting that the influence of mechanical impact is likely in play (entries 5–6). Not surprisingly, when 5 mol% of **2a** was applied, a respectable 88% of **5a** could still be obtained (entry 7). However, when the cage catalyst loading was lowered to 1 mol%, the conversion to the coupling product was hampered (entry 7).

Different kinds of $\mathbf{Pd_2L_2}$ catalysts were also examined in reactions between **3a** and **4** (entries 8–10). With a less sterically congested ethylenediamine (eda) ligand, the catalytic activity of **2b** is vastly diminished, and only 54% of **5a** was achieved (entry 8). On the other hand, **2c**, equipped with a conformationally rigid cyclohexyldiamine, is expected to firmly maintain the L-shaped guest binding pocket, providing **5a** in 93% yield (entry 9). By swapping **L3** with **L4**, **2d** behaved as an excellent confinement catalyst and gave **5a** in 96% yield (entry 10). As a comparison, the catalysis was also examined with capsule $(tmedaPd)_{2L34}$ (**1a**) (65% yield, entry 11). However, control experiments showed that **1** is unstable under mechanochemical conditions and undergoes decomposition, with 58% of **1** remaining after milling at 30 Hz for 30 min (Fig. S41). As such, we attributed the formation of **5a** to base catalysis, as **L3** and **L4** were confirmed to be capable catalysts for the formation of **5a** (entry 14). In comparison, Pd–N_{py} bonds in metallacycle **2a** are stable and unsusceptible to mechanical impact, presumably due to the low strain associated with a nonporous structure. **2a** remains structurally intact under mechanochemical conditions, being quantitatively recovered after milling treatment (Fig. S42). Therefore, we ruled out the possibility that efficient catalysis occurs due to the exposure of Lewis basic pyridyl groups upon ball-milling treatment of $\mathbf{Pd_2L_2}$ catalysts (**2**).

This claim is further supported by the use of $(py)_2PdCl_2$ or $(tmeda)Pd(NO_3)_2$ as catalysts, which produced **5a** in 9% and 2%, respectively (Table 1, entry 13), roughly the same as the background reaction (Table 1, entry 12). Finally, reactions were also carried out under solution-based conditions with **2a** in DMSO-d_6 or in a mixed solution (CD_3CN/D_2O) (entry 15). Although 71% yield of **5a** was achieved, **5a** would have formed even without **2a**, suggesting that a strong background reaction was operative with Lewis-basic DMSO-d_6 or D_2O.

With these optimized conditions in hand, the scope of **2a** as a solid-state catalyst was examined with a series of β-nitrostyrene derivatives **3** and **4** (Fig. 5). Among them, aryls with neutral (**3b**), electron-withdrawing (**3c–f**), and electron-donating groups (**3g–h**) were all tolerated and delivered excellent conversions (>95% yield of **5**).

A unique aspect of enzymes is their tremendous molecular recognition ability, enabling them to carry out catalysis both

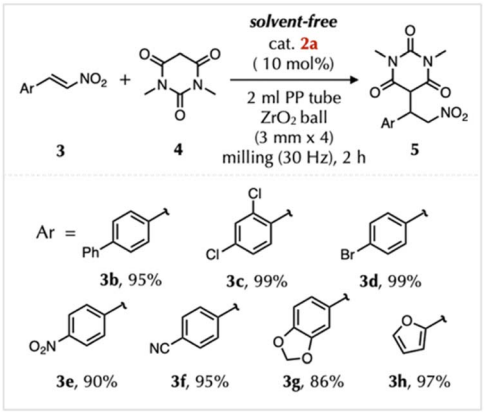

Fig. 5 The solid substrate scope in the mechanochemical Michael addition reaction between 3 and 4 with 2a as a catalyst. Yields were determined using NMR with an internal standard.

efficiently and with high stereo- and regioselectivity.[31] Such a level of recognition is still difficult to achieve with synthetic counterparts. Substrate size and shape recognition is fundamentally important as these properties are typically hard to differentiate with conventional organic or organometallic catalysts. We envisioned that aggregation of **2** would *in situ* generate a cavity space that imposes specific size and shape requirements on the incoming guest molecules. If the size and shape of the cavity match those of the substrate, the substrate would be captured and transformed to the final products. If not, either the transformation would not happen or would be much slower.

Although Michael addition of either **3a** or **3b** with **4** independently led to >95% conversion with metallacycle catalyst **2a** by ball-milling, when they were charged in a one-pot mixture (**3a** + **3b** + **4**) with a catalytic amount of **2a** (10 mol%), coupling products **5a** and **5b** were obtained in 79% and 22% yield, respectively (Fig. 6). Similarly, catalyst **2d** provided **5a** (81%) and **5b** (24%) with similar selectivity under the same milling conditions (Fig. 6a). The use of *N*-methylimidazole (**6a**), a common organic base, would lead to equivalent amounts of **5a** (61%) and **5b** (45%) (Fig. 6). Notably, although the basicity of **6a** is higher than that of **L3** or **L4**, the latter surprisingly gave lower catalytic activity in the Michael addition reaction between **3** and **4**. To reason these confusing results, emission experiments were carried out with milled samples containing **L3** and **G3** and it was found that the emission of **G3** was enhanced (Fig. S40d–f), in sharp contrast to the emission quenching phenomenon observed with **2a** (Fig. 4e). This may suggest that the

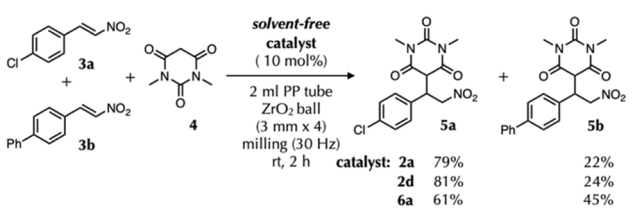

Fig. 6 Substrate size/shape recognition catalysis with 2a, 2d, and organic base 6a.

"compactness" of pyrene aggregation is potentially enhanced to magnify the "excimer" character of **G3**. The unique interaction between **L3** and **G3** might provide insight into why these control reactions with tridentate ligands (**L3** and **L4**) provide such good catalytic results (Table 1, entry 14).

These experiments suggest a certain level of size/shape recognition with $\mathbf{Pd_2L_2}$ catalysts in the solid-state. This is remarkable as most supramolecular systems that exhibit similar size/shape molecular recognition properties are discrete molecular structures.[32] Although the concept of employing discrete cage fragments in self-assembly with guest molecules shares some similarity with the "aromatic micelle" idea pioneered by Lee[33] and Yoshizawa[34] using either ionic or amphiphilic aromatic surfactants, the host–guest behavior of the two approaches is very different. The host–guest chemistry with aromatic surfactants is dictated by the size of guests. In our case, host–guest complexation is instead dictated by the shape of **2**, and this, we believe, is the chemical origin of its unique molecular recognition ability.

Conclusions

In this work we present a family of bent metallacycles (**2**) that can be readily synthesized *via* solvent-free mechanochemistry. Crystallographic analysis revealed the formation of non-covalent capsular assemblies in the solid state, exhibiting varying degrees of structural tightness. Specifically, **2a** forms loosely packed capsules, whereas **2d** self-assembles into tightly packed capsules. Regardless of their static solid-state structures, these assemblies were demonstrated to function as capable hosts for small molecules under mechanical stimulation in the solid-state, hinting at the importance of force to drive these complexation processes. The mechanism would be further examined in depth in the near future in our laboratory. In addition, these $\mathbf{Pd_2L_2}$ metallacycles were further shown to function as confinement catalysts in Michael addition reactions, exhibiting distinctive molecular recognition. This study represents the first mechanochemical approach to confinement catalysis driven by coordination complexes. We anticipate that our non-covalent coordination capsule strategy, inspired by the self-assembly processes of biological macromolecules mediated by non-covalent interactions, will serve as a complementary approach to conventional coordination self-assembly methods for constructing porous coordination structures.

Author contributions

This work was conceptualized by K. Y. All experiments were conducted by P.·W., F.-Z. L. and S. L. The manuscript was written by K. Y. with input from all the authors. All authors have given approval to the final version of the manuscript.

Conflicts of interest

There are no conflicts to declare.

Data availability

CCDC 2378017 and 2403440 contain the supplementary crystallographic data for this paper.[35a,b]

The data supporting this article have been included as part of the supplementary information (SI). Supplementary information is available. See DOI: https://doi.org/10.1039/d5mr00075k.

Acknowledgements

This work was supported by the National Natural Science Foundation of China (22471170), the National Natural Science Foundation of Shanghai (24ZR1452200), and the ShanghaiTech University start-up fund. We also thank other staff members at the Analytical Instrumentation Center of SPST, and ShanghaiTech University (contract no. SPST-AIC10112914) for characterization support.

Notes and references

1 (*a*) D. J. Cram, *Angew Chem. Int. Ed. Engl.*, 1988, **27**, 1009; (*b*) C. J. Pedersen, *Angew Chem. Int. Ed. Engl.*, 1988, **27**, 1021; (*c*) J.-M. Lehn, *Angew Chem. Int. Ed. Engl.*, 1988, **27**, 89.

2 (*a*) J.-P. Sauvage, *Angew. Chem., Int. Ed.*, 2017, **56**, 11080; (*b*) J. F. Stoddart, *Angew. Chem., Int. Ed.*, 2017, **56**, 11094; (*c*) B. L. Feringa, *Angew. Chem., Int. Ed.*, 2017, **56**, 11060.

3 (*a*) G. W. Orr, L. J. Barbour and J. L. Atwood, *Science*, 1999, **285**, 1049; (*b*) Q. He, M. Kelliher, S. Bähring, V. M. Lynch and J. L. Sessler, *J. Am. Chem. Soc.*, 2017, **139**, 7140; (*c*) S. Kennedy, G. Karotsis, C. M. Beavers, S. J. Teat, E. K. Brechin and S. J. Dalgarno, *Angew. Chem., Int. Ed.*, 2010, **49**, 4205.

4 (*a*) T. Heinz, D. M. Rudkevich and J. Rebek Jr, *Nature*, 1998, **394**, 764; (*b*) P. Jacopozzi and E. Dalcanale, *Angew Chem. Int. Ed. Engl.*, 1997, **36**, 613; (*c*) T. Haino, M. Kobayashi, M. Chikaraishi and Y. Fukazawa, *Chem. Commun.*, 2005, **18**, 2321; (*d*) J. C. Sherman, C. B. Knobler and D. J. Cram, *J. Am. Chem. Soc.*, 1991, **113**, 2194; (*e*) X. Liu, Y. Liu, G. Li and R. Warmuth, *Angew. Chem., Int. Ed.*, 2006, **45**, 901; (*f*) J. H. Jordan and B. C. Gibb, *Chem. Soc. Rev.*, 2015, **44**, 547; (*g*) M. Chwastek, P. Cmoch and A. Szumna, *Angew. Chem., Int. Ed.*, 2021, **60**, 4540.

5 (*a*) D. J. Cram, M. E. Tanner, S. J. Keipert and C. B. Knobler, *J. Am. Chem. Soc.*, 1991, **113**, 8909; (*b*) T. Brotin and J.-P. Dutasta, *Chem. Rev.*, 2009, **109**, 88.

6 (*a*) A. Harada, J. Li and M. Kamachi, *Nature*, 1993, **364**, 516; (*b*) C. Kogame-Asahara, S. Ito, H. Iguchi, A. Kazama, H. Shigemitsu and T. Kida, *Chem. Commun.*, 2020, **56**, 1353; (*c*) I. Roy and J. F. Stoddart, *Acc. Chem. Res.*, 2021, **54**, 1440.

7 (*a*) T. Ogoshi, S. Kanai, S. Fujinami, T.-A. Yamagishi and Y. Nakamoto, *J. Am. Chem. Soc.*, 2008, **130**, 5022; (*b*) D. Cao, Y. Kou, J. Liang, Z. Chen, L. Wang and H. Meier, *Angew. Chem., Int. Ed.*, 2009, **48**, 9721; (*c*) M. Guo, X. Wang, C. Zhan, P. Demay-Drouhard, W. Li, K. Du, M. A. Olson, H. Zuilhof and A. C.-H. Sue, *J. Am. Chem. Soc.*, 2018, **140**, 74; (*d*) T. Ogoshi, T.-A. Yamagishi and Y. Nakamoto, *Chem. Rev.*, 2016, **116**, 7937.

8 (*a*) Y. Liu, H. Wang, L. Shangguan, P. Liu, B. Shi, X. Hong and F. Huang, *J. Am. Chem. Soc.*, 2021, **143**, 3081–3085; (*b*) Y. Wu, J. Zhou, E. Li, M. Wang, K. Jie, H. Zhu and F. Huang, *J. Am. Chem. Soc.*, 2020, **142**, 19722; (*c*) B. Wang, Z.-X. Li, H.-N. Wu, Z.-Y. Ning, P.-F. Ju, Y. Liu, Z.-Y. Zhang and C. Li, *Chem.–Eur. J.*, 2025, **31**, e202404566; (*d*) Z. Li and Y.-W. Yang, *Adv. Mater.*, 2022, **34**, 2107401; (*e*) L. Chen, Y. Cai, W. Feng and L. Yuan, *Chem. Commun.*, 2019, **55**, 7883; (*f*) B. Alhazmi, G. Ignacz, M. Di Vincenzo, M. N. Hedhili, G. Szekely and S. P. Nunes, *Nat. Commun.*, 2024, 7151; (*g*) Q. Lin, X. Ding, Y. hou, W. Ali, Z. Li, X. Han, Z. Meng, Y. Sun and Y. Li, *Eco-Environ. Health*, 2024, **3**, 381.

9 (*a*) Q. Duan, Y. Cao, Y. Li, X. Hu, T. Xiao, C. Lin, Y. Pan and L. Wang, *J. Am. Chem. Soc.*, 2013, **135**, 10542; (*b*) D. G. Jimenez, V. Poongavanam and J. Kihlberg, *J. Med. Chem.*, 2023, **66**, 5377; (*c*) E. M. Driggers, S. P. Hale, J. Lee and N. K. Terrett, *Nat. Rev. Drug Discovery*, 2008, **7**, 608.

10 (*a*) C. Wang, L. Xu, Z. Jia and T.-P. Loh, *Chin. Chem. Lett.*, 2024, **35**, 109075; (*b*) D. Zhang, L. Wang, W. Wu, D. Cao and H. Tang, *Chem. Commun.*, 2025, **61**, 599.

11 M. Fujita, J. Yazaki and K. Ogura, *J. Am. Chem. Soc.*, 1990, **112**, 5645.

12 M. Fujita, M. Tominaga, A. Hori and B. Therrien, *Acc. Chem. Res.*, 2005, **38**, 369.

13 (*a*) S. L. James, C. J. Adams, C. Bolm, D. Braga, P. Collier, T. Friščić, F. Grepioni, K. D. M. Harris, G. Hyett, W. Jones, A. Krebs, J. Mack, L. Maini, G. Orpen, I. P. Parkin, W. C. Shearouse, J. W. Steed and D. C. Waddell, *Chem. Soc. Rev.*, 2012, **41**, 413; (*b*) K. J. Ardila-Fierro and J. G. Hernández, *ChemSusChem*, 2021, **14**, 2145; (*c*) E. Colacino, V. Isoni, D. Crawford and F. García, *Trends Chem.*, 2021, **3**, 335; (*d*) J. L. Howard, Q. Cao and D. L. Browne, *Chem. Sci.*, 2018, **9**, 3080; (*e*) D. Virieux, F. Delogu, A. Porcheddu, F. García and E. Colacino, *J. Org. Chem.*, 2021, **86**, 13885; (*f*) F. León and F. García in *Comprehensive Coordination Chemistry III*, ed. E. C. Constable, G. Parkin and L. Que Jr, Elsevier, Amsterdam, 2021, pp. 620–679; (*g*) R. Liu, X. He, T. Liu, X. Wang, Q. Wang, X. Chen and Z. Lian, *Chem.–Eur. J.*, 2024, e202401376; (*h*) K. Kubota and H. Ito, *Trends Chem.*, 2020, **2**, 1066.

14 Selected examples of mechanochemical organic macrocycle synthesis: (*a*) J. Antesberger, G. W. V. Cave, M. C. Ferrarelli, M. W. Heaven, C. L. Raston and J. L. Atwood, *Chem. Commun.*, 2005, 892; (*b*) B. A. Roberts, G. W. V. Cave, C. L. Raston and J. L. Scott, *Green Chem.*, 2001, **3**, 280; (*c*) S. Kaabel, R. S. Stein, M. Fomitšenko, I. Järving, T. Friščić and R. Aav, *Angew. Chem., Int. Ed.*, 2019, **58**, 6230; (*d*) S. Santra, D. S. Kopchuk, I. S. Kovalev, G. V. Zyryanov, A. Majee, V. N. Charushin and O. N. Chupakhin, *Green Chem.*, 2016, **18**, 423; (*e*) E. Suut-Tuule, E. Shults, T. Jarg, J. Adamson, D. Kananovich and R. Aav, *ChemSusChem*, 2025, e202402354.

15 A. Orita, L. Jiang, T. Nakano, N. Ma and J. Otera, *Chem. Commun.*, 2002, 1362.
16 Another example of mechanochemical coordination self-assembly: C. Giri, P. K. Sahoo, R. Puttreddy, K. Rissanen and P. Mal, *Chem.–Eur. J.*, 2015, **21**, 6390.
17 (*a*) Y. Liu, F.-Z. Liu and K. Yan, *Angew. Chem., Int. Ed.*, 2022, e202116980; (*b*) Y. Liu, F.-Z. Liu, S. Li, H. Liu and K. Yan, *Chem.–Eur. J.*, 2023, e202302563.
18 (*a*) M. Yoshizawa, M. Tamura and M. Fujita, *Science*, 2006, **312**, 251; (*b*) M. D. Pluth, R. G. Bergman and K. N. Raymond, *Science*, 2007, **316**, 85; (*c*) V. F. Slagt, J. N. H. Reek, P. C. J. Kamer and P. W. N. M. van Leeuwen, *Angew. Chem., Int. Ed.*, 2001, **40**, 4271; (*d*) W. Cullen, M. C. Misuraca, C. A. Hunter, N. H. Williams and M. D. Ward, *Nat. Chem.*, 2016, **8**, 231; (*e*) L.-D. Syntrivanis, I. Némethová, D. Schmid, S. Levi, A. Prescimone, F. Bissegger, D. T. Major and K. Tiefenbacher, *J. Am. Chem. Soc.*, 2020, **142**, 5894; (*f*) D. Samanta, S. Mukherjee, Y. P. Patil and P. S. Mukherjee, *Chem.–Eur. J.*, 2012, **18**, 12322; (*g*) K. G. Andrews, *Beilstein J. Org. Chem.*, 2025, **21**, 421.
19 (*a*) An analogous $\mathbf{Pd_2L_2}$ species was previously reported by solution-based conditions, see ref. 19b;; (*b*) V. Martí-Centelles, F. Duarte and P. J. Lusby, *Isr. J. Chem.*, 2019, **59**, 257.
20 Notable examples of employing ligand bent angle as a tunable motif for self-assembly design principle: (*a*) Q.-F. Sun, J. Iwasa, D. Ogawa, Y. Ishido, S. Sato, T. Ozeki, Y. Sei, K. Yamaguchi and M. Fujita, *Science*, 2010, **328**, 1144; (*b*) D. Fujita, Y. Ueda, S. Sato, N. Mizuno, T. Kumasaka and M. Fujita, *Nature*, 2016, **540**, 563.
21 (*a*) S. Ghorai and R. Natarajan, *Small*, 2024, **20**, 2400842; (*b*) S. Du, S. Sun, Z. Ju, W. Wang, K. Su, F. Qiu, X. Yu, G. Xu and D. Yuan, *Adv. Sci.*, 2024, **11**, 2308445; (*c*) S. Kumar, T. Lis, W. Bury, P. J. Chmielewski, M. Garbicz and M. Stepień, *Angew. Chem., Int. Ed.*, 2024, **63**, e202316243; (*d*) Q.-H. Guo, Z. Liu, P. Li, D. Shen, Y. Xu, M. R. Ryder, H. Chen, C. L. Stern, C. D. Malliakas, X. Zhang, L. Zhang, Y. Qiu, Y. Shi, R. Q. Snurr, D. Philp, O. K. Farha and J. F. Stoddart, *Chem*, 2019, **5**, 2353; (*e*) Z. Yao, Z. Song, S. Yin, W. Huang, T. Gao, P. Yan, Z. Zhou and H. Li, *Chem.–Eur. J.*, 2025, **31**, e202403976; (*f*) M.-M. Gan, Z.-E. Zhang, X. Li, F. E. Hahn and Y.-F. Han, *Chin. Chem. Lett.*, 2025, **36**(10), 110624; (*g*) Q. Bai, Y.-M. Guan, T. Wu, Y. Liu, Z. Zhai, Q. Long, Z. Jiang, P. Su, T.-Z. Xie, P. Wang and Z. Zhang, *Angew. Chem., Int. Ed.*, 2023, **62**, e202309027; (*h*) M.-H. Du, D.-H. Wang, L.-W. Wu, L.-P. Jiang, J.-P. Li, L.-S. Long, L.-S. Zheng and X.-J. Kong, *Angew. Chem., Int. Ed.*, 2022, **61**, e202200537.
22 X.-Q. Guo, L.-P. Zhou, S.-J. Hu, L.-X. Cai, P.-M. Cheng and Q.-F. Sun, *J. Am. Chem. Soc.*, 2021, **143**, 6202.
23 Despite the low solubility of **G2** in CD_3CN/D_2O (1 : 4), a clear upfield shifted signal of encapsulated **G2** was observed, as shown in Fig. S34. Therefore, the encapsulation of **G2** with **2a** was supported in the solution process.
24 Examples of fluorocarbon encapsulation by coordination confinements range from ~0.1–1.5 ppm. See ref. 25.
25 (*a*) C. R. P. Fulong, M. G. E. Guardian, D. S. Aga and T. R. Cook, *Inorg. Chem.*, 2020, **59**, 6697; (*b*) H. Takezawa, T. Murase, G. Resnati, P. Metrangolo and M. Fujita, *J. Am. Chem. Soc.*, 2014, **136**, 1786.
26 Q. Li and Z. Li, *Adv. Sci.*, 2017, **4**, 1600484.
27 H. Ito, M. Muromoto, S. Kurenuma, S. Ishizaka, N. Kitamura, H. Sato and T. Seki, *Nat. Commun.*, 2012, **4**, 2009.
28 (*a*) O. M. Berner, L. Tedeschi and D. Enders, *Eur. J. Org Chem.*, 2002, **2002**, 1877; (*b*) W. Notz, F. Tanaka and C. F. Barbas III, *Acc. Chem. Res.*, 2004, **37**, 580.
29 (*a*) I. A. Bhat, A. Devaraj, P. Howlader, K.-W. Chi and P. S. Mukherjee, *Chem. Commun.*, 2018, **54**, 4814; (*b*) P. Howlader and P. S. Mukherjee, *Chem. Sci.*, 2016, **7**, 5893; (*c*) P. Howlader, P. Das, E. Zangrando and P. S. Mukherjee, *J. Am. Chem. Soc.*, 2016, **138**, 1668.
30 (*a*) P. K. Boaler, T. K. Piskorz, L. E. Bickerton, J. Wang, F. Duarte, G. C. Lloyd-Jones and P. J. Lusby, *J. Am. Chem. Soc.*, 2024, **146**, 19317; (*b*) R. G. DiNardi, S. Rasheed, S. S. Capomolla, M. H. Chak, I. A. Middleton, L. K. Macreadie, J. P. Violi, W. A. Donald, P. J. Lusby and J. E. Beves, *J. Am. Chem. Soc.*, 2024, **146**, 21196; (*c*) J. Wang, T. A. Young, F. Duarte and P. J. Lusby, *J. Am. Chem. Soc.*, 2020, **142**, 17743.
31 A. Warshel, P. K. Sharma, M. Kato, Y. Xiang, H. Liu and M. H. M. Olsson, *Chem. Rev.*, 2006, **106**, 3210.
32 (*a*) M. Morimoto, S. M. Bierschenk, K. T. Xia, R. G. Bergman, K. N. Raymond and F. D. Toste, *Nat. Catal.*, 2020, **3**, 969; (*b*) C. J. Brown, F. D. Toste, R. G. Bergman and K. N. Raymond, *Chem. Rev.*, 2015, **115**, 3012.
33 T. Zheng, L. Tan, M. Lee, Y. Li, E. Sim, M. Lee and M. J, *J. Am. Chem. Soc.*, 2024, **146**, 25451.
34 (*a*) K. Kondo, A. Suzuki, M. Akita and M. Yoshizawa, *Angew. Chem., Int. Ed.*, 2013, **52**, 2308; (*b*) M. Yoshizawa and L. Catti, *Proc. Jpn. Acad., Ser. B*, 2023, **99**, 29.
35 (*a*) CCDC 2378017: Experimental Crystal Structure Determination, 2025, DOI: 10.5517/ccdc.csd.cc2ktj75; (*b*) CCDC 2403440: Experimental Crystal Structure Determination, 2025, DOI: 10.5517/ccdc.csd.cc2lnzbl.